Micro-WEDM of Ni55.8Ti shape memory superalloy: experimental investigation and optimisation

Hassan Ali M. Meshri

Department of Manufacturing Engineering,
Atilim University,
Incek, 06836, Ankara, Turkey
Email: Hassaninvestor@gmail.com

Samet Akar*

Department of Mechanical Engineering,
Çankaya University,
06790, Ankara, Turkey
Fax: +90 (312) 233 1300
Email: samet.akar@cankaya.edu.tr
*Corresponding author

Mirsadegh Seyedzavvar

Faculty of Engineering,
Adana Alparslan Turkeș University of Science and Technology,
01250, Adana, Turkey
Email: mseyedzavvar@atu.edu.tr

Sadik Engin Kiliç

Department of Manufacturing Engineering,
Atilim University,
Incek, 06836, Ankara, Turkey
Email: engin.kilic@atilim.edu.tr

Abstract: Nickel-titanium superalloy has gained significant acceptance for engineering applications as orthotropic implants, orthodontic devices, automatic actuators, etc. Considering the unique properties of these alloys, such as high hardness, toughness, strain hardening, and development of strain-induced martensite, micro-wire electro-discharge machining (µ-WEDM) process has been accepted as one of the main options for cutting intricate shapes of these alloys in micro-scale. This paper presents the results of a comprehensive study to address the material removal rate (MRR) and surface integrity of Ni55.8Ti shape memory superalloy (SMA) in the µ-WEDM process. The effects of discharge current, pulse on-time, pulse off-time, and servo voltage on the performance of this process, including MRR, white layer thickness, surface roughness, and micro-hardness of the machined surface, were investigated by multi-regression analysis using response surface methodology (RSM). The optimisation of input parameters based on the gradient and the swarm optimisation algorithms were also conducted to maximise the MRR and minimise the white layer thickness, surface roughness, and micro-hardness of the machined samples.

Keywords: $Ni_{55.8}Ti$; µ-WEDM; Kerf; white layer; surface roughness; micro-hardness.

Reference to this paper should be made as follows: Meshri, H.A.M., Akar, S., Seyedzavvar, M. and Kiliç, S.E. (2021) 'Micro-WEDM of Ni55.8Ti shape memory superalloy: experimental investigation and optimisation', *Int. J. Mechatronics and Manufacturing Systems*, Vol. 14, No. 1, pp.18–38.

Biographical notes: Hassan Ali M. Meshri received his BSc in Aeronautical Engineering from Engineering Academy Tajoura in 1998 and MSc in Manufacturing Engineering from Atilim University in 2020. His research focuses on µ-WEDM of shape memory alloys.

Samet Akar is an Assistant Professor of Mechanical Engineering with Çankaya University. He received his BSc from University of Applied Science and Technology in 2005, his MSc from University of Tabriz in 2007, and his PhD from Bilkent University in 2016. His research interests are advanced manufacturing, finite element modelling, and micro-scale design and fabrication.

Mirsadegh Seyedzavvar is an Assistant Professor in Mechanical Engineering with major a manufacturing at Adana Alparslan Türkeş University of Science and Technology. He received his MSc from University of Tabriz for his research on experimental study and FEM of heat transfer and surface integrity of workpiece in electro discharge machining processes. He received his PhD for his work on synthesis and application of eco-friendly nanofluids for abrasive machining. His current research is mainly focused on advanced manufacturing techniques and nanocomposite materials.

Sadik Engin Kiliç received his BSc in Mechanical Engineering, Middle East Technical University, 1972; MSc in Mechanical Engineering (Machine Tool Design), UMIST (University of Manchester Institute of Science and Technology), 1973; PhD in Mechanical Engineering (Machine Tools), 1977. He is Chairman of the Manufacturing Engineering (2013-) and the Acting Chairman of the Mechanical Engineering (2018-) departments at Atılım University. His research focus on metal cutting technology, process dynamics and optimisation, manufacturing systems modelling, flexible, integrated, distributed, virtual and eco systems, and sustainable manufacture.

1 Introduction

The nickel-titanium shape memory superalloys (Nitinol SMAs) possess a lower stress shielding effect and much higher strain recovery than steel alloys, which make them a better choice as biomedical implants, and are more flexible and resistant to cyclic fatigue which are important for mechanical actuators (Wadood, 2016; Kalmar et al., 2019). However, machining of these alloys using conventional metal cutting techniques is very difficult because of their specific properties of high strength, high specific heat, and formation of strain-induced martensite that result in high tool wear and low integrity of machined surfaces (Guo et al., 2013). These characteristics make the wire electrical discharge machining (WEDM) the most appropriate and widely accepted nonconventional machining technique of Nitinol superalloys (Sharma et al., 2017).

However, to produce features in the micro-scale, the μ-WEDM process, which uses lower discharge energies and smaller wire-electrode diameter as compared with the WEDM process, has been introduced (Puri, 2017). The temperature developed during electrical discharges greatly influences the surface integrity characteristics of the Nitinol superalloys, including surface roughness (SR), micro-hardness (μH), and thickness of the re-solidified layer (called white later) (WLT) of the machined workpiece (Daneshmand et al., 2012).

Most of the researches concerning the WEDM of Nitinol SMA relies on the study of the effects of process parameters on the performance of the WEDM process, with no to little reference to the μ-WEDM process (Manjaiah et al., 2015; Hsieh et al., 2009). Manjaiah et al. (2015) investigated the effects of WEDM parameters, including pulse on-time, T_{on} (120–130 μs), pulse off-time, T_{off} (48–62 μs), and servo voltage, SV (20–80 V) on MRR and SR of $Ti_{50}Ni_{50-x}Cu_x$ superalloys. They reported that arithmetic mean roughness (R_a) of 1.83 μm and cutting rate of 7.6 mm/min under optimum process parameters are achievable. The authors also showed the formation of TiO_2 and $NiTiO_3$ phases on the samples because of the high temperature induced during WEDM. Hsieh et al. (2009) studied the effect of T_{on} (1–5μs) on the hardness, SR, and composition of the machined surface of TiNiZr and TiNiCr SMAs in the WEDM process. They showed that the cutting rate (CR), R_a, and WLT increase with increasing T_{on}. The authors also reported the formation of metal oxides, including TiO_2, $TiNiO_3$, Cr_2O_3, and Cu_2O in the recast layer resulted in the higher hardness of this layer as compared with that of the base alloy. The formation of Cu_2O was ascribed to the deposition of Cu atoms from the brass wire on the surface of the workpiece. Soni et al. (2017) conducted experiments to evaluate the effects of T_{on} (105−128 μs), T_{off} (28−56 μs) and SV (20−60 V) on MRR and SR of $Ti_{50}Ni_{40}Co_{10}$ SMA. They reported that MRR and SR both increased with increasing T_{on} and both decreased with increasing T_{off}. The authors found the minimum WLT at low T_{on} and high SV levels.

Furthermore, optimisation techniques have been employed extensively to achieve the discharge parameters that result in maximum MRR and minimum tool wear and SR of the workpiece. In this regard, Upadhyay et al. (2019) investigated the rheological effects of magnetic fluid in the discharge gap of the electro-discharge process induced by the rotational magnetic field on the aluminium particles suspended in the dielectric fluid. The authors optimised the levels of I_d, T_{on}, and discharge duty cycle to maximum the MRR while minimising the R_a of the workpiece. They reported that the repulsion of debris from the discharge gap was improved by the rotational effect of the magnetic field, increasing discharge efficiency and MRR. Agrawal and Kamble (2019) employed RSM central composite design (L_{20}) to understand the effects of etching time, temperature, and concentration of ferric chloride etchant on the MRR and undercut in photochemical machining of SS-304 stainless steel. Sharma et al. (2017) conducted experiments based on RSM central composite rotatable design to identify the influence of WEDM process parameters, including T_{on} (105–124 μs), T_{off} (25–55 μs), SV (30–80 V), and I_d (11–19 A) on the CR, dimensional shift (d_{sf}) and mean surface roughness depth (R_z) of the $Ni_{40}Ti_{60}$ SMA.

The d_{sf} was defined as the gap between the surface and the wire periphery. Rathi et al. (2019) investigated the influence of T_{on} (90–110 μs), T_{off} (20–30 μs), and I_d (2–6A) on response variables of MRR and SR in the WEDM process of $Ni_{55.8}Ti$ SMA. They designed experiments based on Taguchi's L_9 orthogonal array and used Gray relation analysis (GRA) to obtain combined optimal WEDM parameters to maximise CR while minimising SR. The authors reported that I_d was the most significant parameter influencing the MRR and SR. Magabe et al. (2019) conducted experiments based on Taguchi's L_{16} technique to evaluate the effects of T_{on} (0.35–1 μs), T_{off} (9–24 μs), SV (20–50V), and wire feed rate (3–12 m/min) on MRR and SR of $Ni_{55.8}Ti$ SMA in WEDM process and employed the non-dominated sorting algorithm-II (NSGA-II) to obtain the optimal levels of these parameters.

They showed that T_{on} was the most significant factor influencing the MRR and R_z, both of which increased with increasing T_{on}. They showed that the models developed using the NSGA-II algorithm were able to predict the MRR and R_z with maximum errors of 3.43 and 5.08 %, respectively. Chaudhari et al. (2019) used RSM based on Box-Behnken design (BBD) technique to investigate the effects of T_{on} (35–55 μs), T_{off} (10–20 μs), and I_d (2–4A) on MRR, SR, and μH of $Ni_{55.8}Ti$ SMA in WEDM process. They optimised the process parameters using a heat transfer search (HTS) algorithm and validation based on retention of shape memory effect using results of differential scanning calorimetry (DSC) tests. The authors reported that the developed models based on the HTS algorithm were able to predict the response variables with errors of less than 1.5%.

As illustrated in the literature review, the most important input parameters of the WEDM process are T_{on}, T_{off}, I_d, and SV and the major response variables include MRR, SR, and dimensional shift of the machined workpiece. Furthermore, the microscopic changes in the surface characteristics of nitinol SMA after the WEDM process due to induced recast layer, or white layer, on the machined surface are of crucial importance as these changes significantly affect the shape memory and elastic recovery characteristics of these alloys (Chaudhari et al., 2019). As the recast layer exhibits no shape memory effect, the effect of this layer is the depression of the shape memory characteristic of the base metal (Hsieh et al., 2009). Furthermore, the creation of metal oxides on this layer results in the higher hardness of the surface layer and a reduction in the fatigue strength and toughness of the workpiece. The formation of TiO_2 in this layer results in the exhausting of Ti atoms on the surface and diffusion of residual Ni atoms to the sublayer and formation of Ni-rich regions. The overall effect of these phenomena would be a reduction in the elastic recovery and fracture toughness of the machined workpiece (Hsieh et al., 2009, Sharma et al., 2017). The creation of a white layer with a thickness of 18 μm on $Ni_{40}Ti_{60}$ SMA in the WEDM process was also reported by Sharma et al. (2017). The authors showed that the formation of TiC and metal oxides in the white layer raised the hardness of the machined surface to 875 HV, several times greater than the hardness of the base material. Reduction in the shape recovery of $Ni_{60}Ti$ SMA with an increase in the bending strain as compared with that of as annealed alloy before machining due to the formation of metal oxides, such as NiO and Cu_2O, in the recast layer and significant increase of surface hardness as compared with the base alloy in the WEDM process were also reported in the literature (LotfiNeyestanak and Daneshmand, 2013).

Based on the literature review and to the best of our knowledge, there has been no specific report on the WEDM process of nitinol shape memory alloys on a micro-scale. Therefore, to fill this gap current study was aimed to investigate the performance of the μ-WEDM process in the machining of $Ni_{55.8}Ti$ SMA in terms of important machinability features, MRR, and surface integrity of the machined workpiece. The experiments were designed based on L27 Taguchi orthogonal array to reduce the number of experiments. The surface integrity of the machined sample was determined based on the R_a and µH values and WLT induced on the machined surface. Mathematical models were generated for each response variable and the significance of the models and influencing factors were analysed by ANOVA. Electro Diffraction spectroscopy (EDS) of the machined surfaces was conducted to analyse the presence of oxygen or other elements in the machined surface layer. Also, the surface of a typical machined surface was tested using X-ray diffraction spectroscopy (XRD) for the formation of metal oxides in the white layer. Two algorithms, namely gradient algorithm (GA) and particle swarm optimisation (PSO) algorithm were used to determine the optimum levels of input parameters to obtain the best levels of response variables, maximising the MRR and minimising the WLT and R_a of the machined samples, individually and simultaneously. The models were validated by comparing the results of both algorithms for individual and combined responses.

Therefore, the current study was aimed to investigate the surface integrity of $Ni_{55.8}Ti$ SMA in the µ-WEDM process using Taguchi's L_{27} orthogonal array technique of RSM. Mathematical models were generated for each response variable and the significance of the models and influencing factors were analysed by the analysis of variance (ANOVA). The machined surfaces of samples were tested using X-ray diffraction spectroscopy (XRD) for the formation of metal oxides in the white layer.

Two algorithms, namely gradient algorithm (GA) and PSO algorithm were used to determine the optimum levels of input parameters to obtain the maximum MRR minimum levels of WLT, SR, and µH.

2 Experimental process, design, and optimisation

2.1 Experimental procedure and equipment

A sample of $Ni_{55.8}Ti$ SMA with the dimensions of 60 × 10 × 5 mm was prepared for the µ-WEDM experiments and 9 slots were cut under different cutting parameters as depicted in Figure 1. A high-precision Sodick AP250L wire electro-discharge machine, with a 100 µm diameter brass wire as the tool and EDM fluid 108 MP-S as the dielectric liquid, was used to conduct the µ-WEDM experiments.

Figure 1 The $Ni_{55.8}Ti$ SMA sample and cutting kerfs in µ-WEDM experiments (see online version for colours)

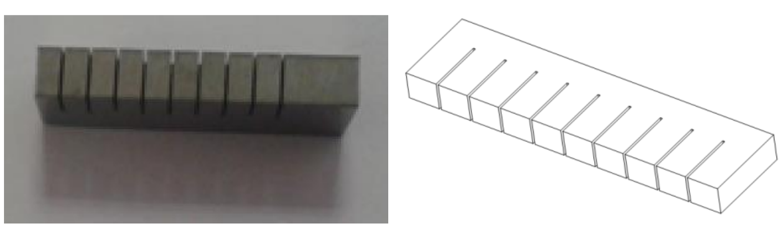

Four parameters, namely pulse on-time (T_{on}), pulse off-time (T_{off}), servo voltage (SV), and discharge current (I_d) were specified as the process parameters. The range of each parameter was determined from the preliminary experiments (Table 1). The MRR was determined as a function of the Kerf width (KW), the workpiece thickness (t), and the cutting rate (CR) using equation (1) The KW was measured from microscopic images of the cutting kerf obtained using Leica DMi8 M/C/A invert light microscope Figure 2. An average of ten readings at different 10 spots along the cutting length of the sample was reported as the KW for each kerf.

$$MRR = KW \times t \times CR \quad (1)$$

To conduct microscopic examinations of the cutting section to determine WLT, the samples went through a preparation procedure of mounting in epoxy, grinding using sandpapers, polishing and etching. For this purpose, grinding was performed on the samples with 800, 1000, and 2500 grade silicon carbide sandpapers. Polishing was performed using two suspension liquids of aluminium oxide (AI_2O_3) (average size 1 µ) and diamond (average size 0.3 µ) particles. The etching of the samples was performed on the cross-section of the machined surface in a solution composed of 10 ml HF, 20 ml HNO_3 and 30 ml HO_2 (Es-Souni et al., 2002). The scanning electron microscope was a Quanta 200f SEM system equipped with an electron dispersive spectroscopy (EDS) unit. X-ray diffraction analyses were conducted using a Philips XRD spectrometer with CuK_α radiation.

Table 1 µ-WEDM input parameters and their levels

	Level		
Parameter	*I*	*II*	*III*
T_{on} (µs)	3.5	5	7.5
T_{off} (µs)	5	10	16
I_d (A)	0.6	6	11
SV (V)	80	130	180

Figure 2 Representation of cutting kerf in the µ-WEDM process: (a) schematic representation and (b) the microscopic image at machining parameters of T_{on} = 5 µs, T_{off} = 10 µs, I_d = 11 A and SV = 80 V

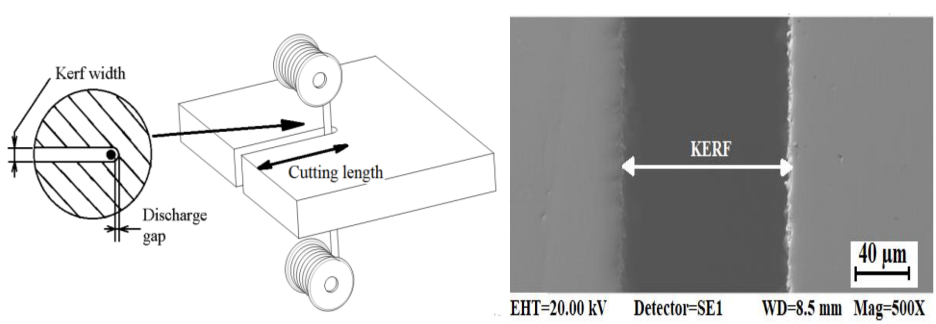

The surface roughness of the samples was measured using a precise confocal laser scanning microscopy, KEYENCE VK-X110 series, with a 50X magnification lens and a scanning rate of approximately 0.08 µm/s (Figure 3). The surface roughness of the samples was reported using arithmetic mean surface roughness (R_a) measured with a cutoff length of 0.8 µm. An average of surface roughness in four consecutive readings of each machined surface was reported as R_a. The micro-hardness measurements of the machined surfaces were conducted on a ZWICK. ROELL ZHvμ micro-hardness tester using an indenter force of 1 kg applied in 10 s on the sample surface via a 136° pyramidal diamond indenter.

Figure 3 Surface roughness measurement: (a) KEYENCE Vk-x100 confocal laser scanning microscopy and (b) surface topography of machined surface at T_{on} = 5 μs, T_{off} = 10 μs, I_d = 11 A and SV = 80 V (see online version for colours)

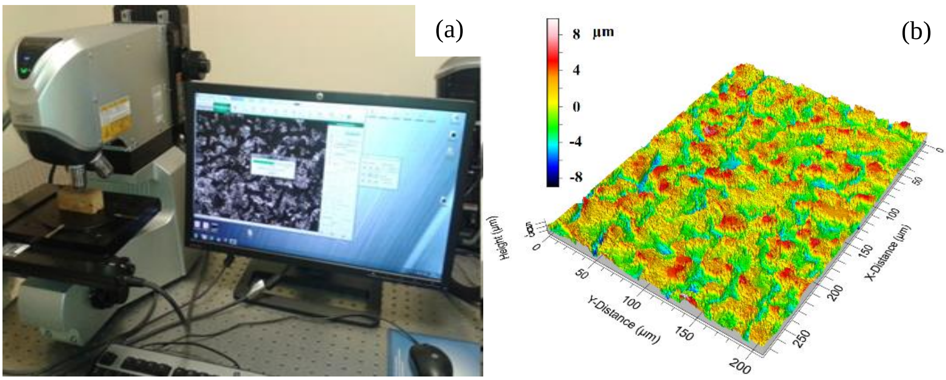

2.2 *Design of experiments and response surface methodology*

The design of experiments was conducted using the Taguchi orthogonal array (L_{27}) technique. The experiments were repeated three times for each set of parameters and an average of measurements were reported as the response variables of the μ-WEDM process. The RSM based on the desirability function approach was applied to generate the regression models of the response variables with a confidence level of 95% using Minitab software. The ANOVA was performed to evaluate the adequacy of the regression model and the significance of each parameter on the response variables (Roy and Kumar, 2014).

2.3 *Optimisation analyses approach*

The gradient and the PSO algorithms were used to identify the optimal levels of input parameters to maximise the MRR and minimise the WLT, SR, and μH in μ-WEDM of $Ni_{55.8}Ti$ SMA. A comparison of the results of these algorithms was used to validate the accuracy of the models developed based on each algorithm.

2.3.1 *Gradient algorithm*

The GA was used to transform the individual or combined responses into desirability indices based on the following steps (Majumder et al., 2014).

Step 1: The individual desirability index (y_i) was calculated for each response variable according to the required state of the response, either to increase or decrease the response or to achieve a specific target. For the state of response to achieve the minimum, equation (2) was used.

$$\left.\begin{array}{ll} y_i = 0 & i > H_i \\ y_i = \left[\left(H_i - i\right)/\left(H_i - S_i\right)\right]^{ri} & S_i \le i \le L_i \\ y_i = 1 & i < S_i \end{array}\right\} \tag{2}$$

where i is the predicted value, S_i is the smallest acceptable value, and H_i is the highest acceptable value of the ith response, respectively. r^i is the weight exponent.

Step 2: The y_i indices were combined according to equation (3) to achieve the global desirability index (D). To obtain the highest quality characteristics by selecting the optimal setting of µ-WEDM parameters, the D index should be maximised or in other words, the fitness function, Y defined by equation (4), should be minimised.

$$D = \left(y_1^{w_1} * y_2^{w_1} * \cdots * y_n^{w_n}\right)^{1/\sum_{j=1}^{n} w_j} \tag{3}$$

$$Y = \frac{1}{1 + D} \tag{4}$$

where n is the total number of response parameters and w_i is the individual weight of the jth response.

2.3.2 Particle swarm optimisation (PSO) algorithm

The PSO is a random arithmetic search and modulation method that relies on the movement and intelligence of swarms to find items while searching for specific targets within a specific search space (Al-Anzi and Allahverdi, 2007). The idea of the algorithm is based on the solutions provided by each of the swarms. Each of these solutions, termed as 'particle', searches space of its quest, looking for the optimal position to land.

This particle has a memory of tracking and remembering the best position reached in the past. In PSO, there is a combination of the local experience (particle's self-experience) and the global experience (the experience of neighbouring particles) that provides the optimal solution within the search space over time (Júnior et al., 2018).

In this study, three different processes of the PSO category, namely PSO-original (PSO-O), PSO-inertia weight (PSO-IW), and PSO-constriction factor (PSO-CF), were used based on the desirability model generated by the RSM to predict the optimum parameter levels to MRR, WLT, SR, and µH (Fourie and Groenwold, 2002). The steps used in the algorithm are shown in Figure 4.

Assuming that the swarms search for a certain goal in a specific d-dimensional space, the position and velocity of the ith particle in this space could be represented by d-dimensional position $x_i = (x_{i1}, x_{i2}, \ldots, x_{id})$ and velocity $v_i = (v_{i1}, v_{i2}, \ldots, v_{id})$ vectors, respectively. Moreover, considering the best-visited position of the ith particle as p_{id} and the best position explored so far as g_{id}, the updating rules of position and velocity based on these three methods are as follows. These rules were employed to develop the PSO by coding in MATLAB.

Figure 4 Flow chart of particle swarm optimisation algorithm

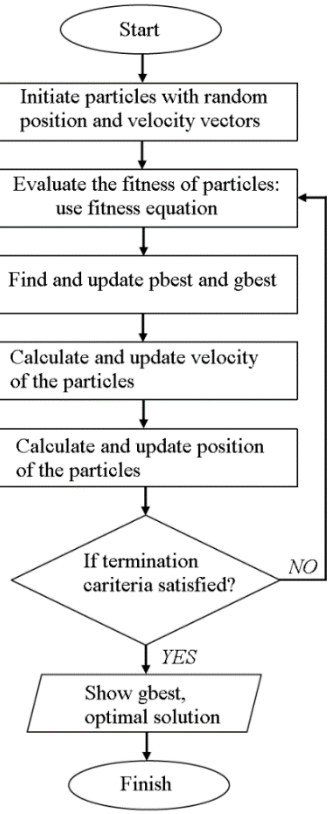

Source: Júnior et al. (2018)

2.3.2.1 *PSO-Original (PSO-O)*

At the initial stage of development, the velocity and position of each particle are determined as follows:

$$v_{id}^{j+1} = v_{id}^{j} + c_1 \times r_1 \left(p_{id} - x_{id}^{j} \right) + c_2 \times r_2 \left(g_{id} - x_{id}^{j} \right) \quad (5)$$

$$x_{id}^{j+1} = x_{id}^{j} + v_{id}^{j+1} \quad (6)$$

where the cognitive parameter $C_1 = 2$, the social parameter $C_2 = 2$, r_1, and r_2 are random numbers uniformly distributed in the range [0–1], and $j = 1, 2\ldots$ is the current iteration (Bai, 2010).

2.3.2.2 *POS-inertia weight (PSO-IW)*

The new velocity and position of each particle are determined according to the following equations:

$$v_{id}^{j+1} = w \times v_{id}^{j} + c_1 \times r_1 \left(p_{id} - x_{id}^{j} \right) + c_2 \times r_2 \left(g_{id} - x_{id}^{j} \right) \quad (7)$$

$$x_{id}^{j+1} = x_{id}^{j} + v_{id}^{j+1} \tag{8}$$

$$w = w_{max} - \frac{w_{max} - w_{min}}{N_{max}} \times iter \tag{9}$$

where *w* is the inertia weight or the proportional agent, that controls the influence of the last velocity on the current velocity. Generally, '*w*' follows the linear decrease with iteration from 0.9 to 0.4. Therefore, the initial weight $w_{max} = 0.9$, the final weight $w_{min} = 0.4$, and N_{max} is the maximum number of iterations (Bai, 2010).

2.3.2.3 PSO-constriction factor (PSO-CF)

In this method, the new position and velocity of each particle is determined according to the following equations (Clerc, 1999):

$$v_{id}^{j+1} = k\left\{v_{id}^{j} + c_1 \times r_1\left(p_{id} - x_{id}^{j}\right) + c_2 \times r_2\left(g_{id} - x_{id}^{j}\right)\right\} \tag{10}$$

$$x_{id}^{j+1} = x_{id}^{j} + v_{id}^{j+1} \tag{11}$$

$$k = \frac{2}{\left|2 - c - \sqrt{c^2 - 4c}\right|} \tag{12}$$

where *k* is the constriction factor, $C = C_1 + C_2$ (Dhas and Kumanan, 2011).

3 Results and discussion

The results of experiments of the µ-WEDM process of $Ni_{55.8}Ti$ SMA, as averages of measurements conducted under each parameter settings based on the orthogonal Taguchi array L_{27} approach, are represented in Table 2. The results of the ANOVA and optimisation algorithms are provided in the following sections.

Table 2 Results of µ-WEDM experiments based on Taguchi's L_{27} standard orthogonal array

	Input parameters levels				*Measured output responses*				
	T_{on}	T_{off}	I_d	*SV*	*KW*	*MRR*	*WLT*	R_a	*µH*
Exp. No.	*µs*	*µs*	*A*	*V*	*mm*	*mm³/min*	*µm*	*µm*	*Vickers (kg/mm²)*
1	3.5	5	0.6	80	0.242	0.270	4.114	0.331	384.7
2	3.5	5	6	130	0.240	0.363	2.717	0.346	390.5
3	3.5	5	11	180	0.245	0.313	3.609	0.339	405.4
4	3.5	10	0.6	130	0.247	0.217	5.048	0.255	378.5
5	3.5	10	6	180	0.244	0.156	5.494	0.298	396.7
6	3.5	10	11	80	0.237	0.297	4.334	0.323	494.7
7	3.5	16	0.6	180	0.251	0.014	5.496	0.232	261.5
8	3.5	16	6	80	0.237	0.143	3.890	0.306	362.9

Table 2 Results of µ-WEDM experiments based on Taguchi's L_{27} standard orthogonal array (continued)

	Input parameters levels				*Measured output responses*				
	T_{on}	T_{off}	I_d	*SV*	*KW*	*MRR*	*WLT*	R_a	*µH*
Exp. No.	*µs*	*µs*	*A*	*V*	*mm*	*mm³/min*	*µm*	*µm*	*Vickers (kg/mm²)*
9	3.5	16	11	130	0.238	0.272	2.434	0.299	377.7
10	5	5	0.6	80	0.244	0.285	5.090	0.281	518.6
11	5	5	6	130	0.238	0.402	3.188	0.321	536.9
12	5	5	11	180	0.243	0.353	4.080	0.317	551.7
13	5	10	0.6	130	0.245	0.257	5.519	0.234	524.8
14	5	10	6	180	0.242	0.196	5.965	0.276	543.0
15	5	10	11	80	0.236	0.353	4.733	0.295	640.3
16	5	16	0.6	180	0.249	0.054	5.967	0.210	407.8
17	5	16	6	80	0.234	0.183	4.361	0.285	509.2
18	5	16	11	130	0.235	0.312	2.906	0.278	524.1
19	7.5	5	0.6	80	0.246	0.344	5.566	0.322	507.8
20	7.5	5	6	130	0.240	0.462	3.664	0.364	526.1
21	7.5	5	11	180	0.245	0.412	4.556	0.357	540.9
22	7.5	10	0.6	130	0.246	0.316	5.995	0.274	514.0
23	7.5	10	6	180	0.244	0.255	6.441	0.316	532.2
24	7.5	10	11	80	0.237	0.396	5.281	0.342	630.2
25	7.5	16	0.6	180	0.250	0.113	6.443	0.250	397.1
26	7.5	16	6	80	0.236	0.242	4.837	0.323	484.7
27	7.5	16	11	130	0.237	0.371	3.382	0.318	513.3

3.1 ANOVA and optimisation of MRR

The results of the ANOVA of the MRR are shown in Table 3. The regression model constructed with 8 DF using the RSM is provided in equation (13). Since the difference between the R^2 and adj-R^2 was approximately zero, the predictive capability of the regression model was significant. Additionally, the reasonable agreement between the adj-R^2 and the predictive R^2 showed that the experimental and the predicted data of the regression model were identical.

$$\begin{aligned}\text{MRR} = (-0.1987) + 0.03228\ T_{\text{on}} - 0.02140\ T_{\text{off}} + 0.00834\ I_d + 0.008315\ \text{SV} \\ - 0.000748\ T_{on}^2 + 0.000298\ T_{off}^2 + 0.000396\ I_d^2 - 0.000035\ \text{SV}^2\end{aligned} \quad (13)$$

As shown in Table 3, the p-value of less than 0.05 and a large F-value indicated that the regression model was statistically significant. Additionally, judging from the F-values obtained by the ANOVA, the SV, T_{off}, I_d, and T_{on} were the most significant factors affecting the MRR, respectively.

Table 3 ANOVA of material removal rate of test samples

Source	*DF*	*Adj SS*	*Adj MS*	*F*	*P*
Regression	8	0.31743	0.039679	1172.31	0.000
T_{on}	1	0.000686	0.000686	30.27	0.000
T_{off}	1	0.005387	0.005387	159.17	0.000
I_d	1	0.002143	0.002143	63.31	0.000
SV	1	0.037889	0.037889	1119.43	0.000
$T_{on}\times T_{on}$	1	0.000046	0.000046	1.37	0.258
$T_{off}\times T_{off}$	1	0.000479	0.000479	14.14	0.001
$I_d\times I_d$	1	0.000684	0.000684	20.21	0.000
SV×SV	1	0.045290	0.045290	1338.09	0.000
Error	18	0.000609	0.000034		
Total	26	0.318040			

R^2=99.81%, adj-R^2=99.72%, pred-R^2=99.57%.

Furthermore, the results of the GA optimisation to determine the input parameters that lead to the maximum MRR are shown in Figure 5. As shown in this figure, the MRR increases monotonically with increasing T_{on} and I_d while it decreases with an increase in T_{off}. This phenomenon is because of an increase in the discharge energy by an increase in the I_d and T_{on} and a reduction in the frequency of discharges with an increase in the T_{off}. Nevertheless, the MRR shows a maximum value for the SV of 115.35 V and decreases with a further increase in this parameter. This phenomenon is related to the fact that the discharge gap grows with increasing servo voltage, resulting in a larger plasma channel with reduced penetration into the workpiece and a decrease in the flushing efficiency at the end of each discharge (Mu et al., 2018).

Also, the accumulative results of GA and PSO-optimisation techniques of µ-WEDM parameters to achieve the maximum MRR as well as the values calculated by replacing these quantities in equation (13) are shown in Table 4. According to the results, the MRR values obtained by the two optimisation techniques are very close and the difference is almost negligible.

Figure 5 Optimum µ-WEDM parameters to achieve the maximum MRR based on GA (d: composite desirability index) (see online version for colours)

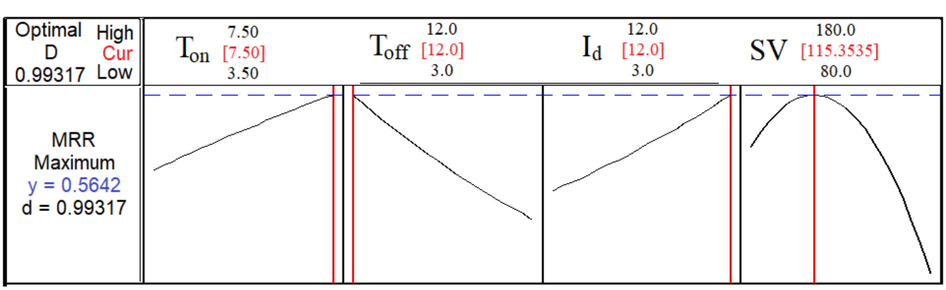

Table 4 Optimum levels of μ-WEDM parameters to obtain maximum material removal rate

Parameters	*d. index = 0.99317*	*PSO*
T_{on} (μs)	7.5	7.5
T_{off} (μs)	5	5
I_d (A)	12	12
SV (V)	115.354	114.96554
MRR (mm^3/min)	0.564219	0.56423

3.2 ANOVA and optimisation of WLT

The results of the ANOVA of the WLT are shown in Table 5. Also, the regression model constructed with 8 DF using the RSM is represented in equation (14). Based on the ANOVA, the difference between the R^2 and adj-R^2 was less than 0.23%,, and the adj-R^2 and the predictive R^2 were very close, demonstrating that the predictive capability of the regression model was significant and the predicted data of this model were consistent.

$$\begin{aligned} \text{WLT} = {} & 5.398 + 0.671\, T_{\text{on}} + 0.8717\, T_{\text{off}} - 0.2180\, I_d - 0.11225\, \text{SV} - 0.0382\, T_{\text{on}}^2 \\ & - 0.040\, T_{\text{off}}^2 + 0.00597\, I_d^2 + 0.000457\, \text{SV}^2 \end{aligned} \tag{14}$$

According to Table 5, the p-value and F-value of the model are 0 and 443.77, respectively, indicating that the regression model was statistically significant. Additionally, judging from the p-values and F-values of the factors, the I_d, SV, T_{on}, and T_{off} were the most significant parameters influencing the WLT, respectively.

Table 5 ANOVA of white layer thickness on the machined surface

Source	*DF*	*Adj SS*	*Adj MS*	*F*	*P*
Regression	8	34.2027	4.27533	443.77	0.000
T_{on}	1	0.2961	0.29610	30.73	0.000
T_{off}	1	8.9388	8.93885	927.84	0.000
I_d	1	1.4638	1.46378	151.94	0.000
SV	1	6.9048	6.90481	716.71	0.000
$T_{on}\times T_{on}$	1	0.1203	0.12031	12.49	0.002
$T_{off}\times T_{off}$	1	8.6184	8.61841	894.58	0.000
$I_d\times I_d$	1	0.1560	0.1560	16.19	0.001
SV×SV	1	7.8220	7.82202	811.91	0.000
Error	18	0.1734	0.00963		
Total	26	34.3761			

R^2=99.50%, adj-R^2=99.27%, pred-R^2=98.86%.

Furthermore, the results of the GA optimisation to determine the input parameters that lead to the minimum WLT are shown in Figure 6. According to this figure, the WLT increases monotonically with increasing T_{on} while there is an opposite pattern for the I_d. This phenomenon could be explained by the fact that the flushing efficiency of the discharge channel decreases with an increase in the T_{on}, resulting in a higher amount of the molten metal resolidified on the surface of the workpiece and larger WLT. In contrast, the flushing efficiency increases with increasing I_d which leads to a reduction in the WLT (Shabgard et al., 2011).

Figure 6 Optimum μ-WEDM parameters to achieve the minimum WLT based on GA (d: Composite desirability index) (see online version for colours)

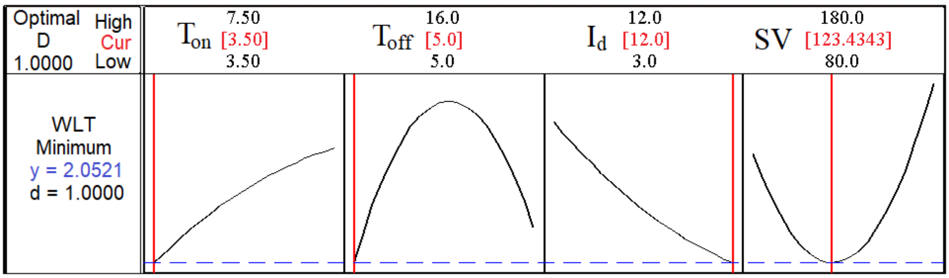

Additionally, the accumulative results of GA and PSO-optimisation techniques to achieve the minimum WLT and the values calculated by replacing these quantities in equation (14) are shown in Table 6. Accordingly, the WLT values calculated based on the two optimisation techniques are the same.

Table 6 Optimum levels of μ-WEDM parameters to obtain minimum white layer thickness

Parameters	*d. index = 0.99317*	*PSO*
T_{on} (μs)	3.5	3.5
T_{off} (μs)	5	5
I_d (A)	12	12
SV (V)	123.434	123.7695
WLT (μm)	2.05212	2.05212

3.3 ANOVA and optimisation of R_a

The results of the ANOVA of the R_a of the machined $Ni_{55.8}Ti$ SMA surfaces are shown in Table 7. Also, the regression model obtained with **8** DF using the RSM is represented in equation (15). Based on the ANOVA, the difference between the R^2 and adj-R^2 was less than 0.62%, and the adj-R^2 and the predictive R^2 were very close, showing that the predictive capability of the regression model was significant and the experimental and the predicted data were consistent.

$$\begin{aligned} R_a &= 0.6048 - 0.08793 T_{on} - 0.01641\, T_{off} + 0.01458\, I_d - 0.000385\ \mathrm{SV} \\ &\quad + 0.008342\, T_{on}^2 + 0.000551\, T_{off}^2 - 0.000815\, I_d^2 + 0.000001 SV^2 \end{aligned} \tag{15}$$

According to Table 7, the p-value and F-value of the model for R_a are 0 and 158.64, respectively, showing that the regression model was statistically significant. Furthermore, judging from the p-values and F-values of the factors, the T_{off}, I_d, SV, and T_{on} were the most significant parameters influencing the R_a, respectively.

Table 7 ANOVA of arithmetic surface roughness of the machined surface

Source	*DF*	*Adj SS*	*Adj MS*	*F*	*P*
Regression	8	0.040039	0.005005	158.64	0.000
T_{on}	1	0.005092	0.005092	161.39	0.000
T_{off}	1	0.003167	0.003167	100.38	0.000
I_d	1	0.006548	0.006548	207.54	0.000
SV	1	0.000081	0.000081	2.58	0.126
$T_{on}\times T_{on}$	1	0.005751	0.005751	182.29	0.000
$T_{off}\times T_{off}$	1	0.001637	0.001637	51.89	0.000
$I_d\times I_d$	1	0.002905	0.002905	92.09	0.000
SV×SV	1	0.000012	0.000012	0.40	0.537
Error	18	0.000568	0.000032		
Total	26	0.040607			

R^2=98.60%, adj-R^2=97.98%, pred-R^2=96.85%.

Furthermore, the results of the GA optimisation to determine the input parameters to minimise the R_a are shown in Figure 7. Accordingly, the R_a decreases monotonically with an increase in T_{off} and SV. This is explainable as an increase in the T_{off} or SV provides better flushing of the cutting debris from the discharge gap by reducing the frequency of the discharges and increasing the discharge gap, respectively. Consequently, the possibility of arc discharges decreases, raising the percentage of normal discharges and improving the surface finish (Kumar et al., 2015). However, the R_a is minimum under specific levels of T_{on} and I_d at which there is a balance between the size of the craters formed on the surface of the workpiece by the successive discharges and the flushing efficiency of the plasma channel at the end of each discharge. Less overlap of the craters and improvement of the surface finish of the machined workpiece by an increase in the T_{off} and SV and decrease in the I_d could be seen in the SEM images in Figure 8.

Figure 7 Optimum µ-WEDM parameters to achieve the minimum WLT based on GA (d: Composite desirability index) (see online version for colours)

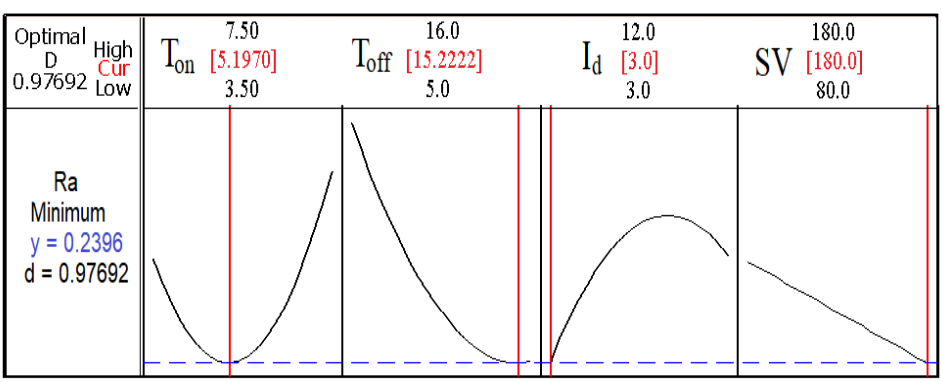

Additionally, the accumulative results of GA and PSO-optimisation techniques to achieve the minimum R_a and the values calculated by replacing these quantities in equation (15) are shown in Table 8. Accordingly, there is high proximity between the R_a values calculated based on the two optimisation techniques.

Figure 8 SEM images of surface topography of $Ni_{55.8}Ti$ SMA after µ-WEDM at; (a, b) T_{on} = 5 µs, T_{off} = 10 µs, I_d = 11 A, SV = 80 V and (c, d) T_{on} = 5 µs, T_{off} = 16 µs, I_d = 0.6 A, SV = 130 V

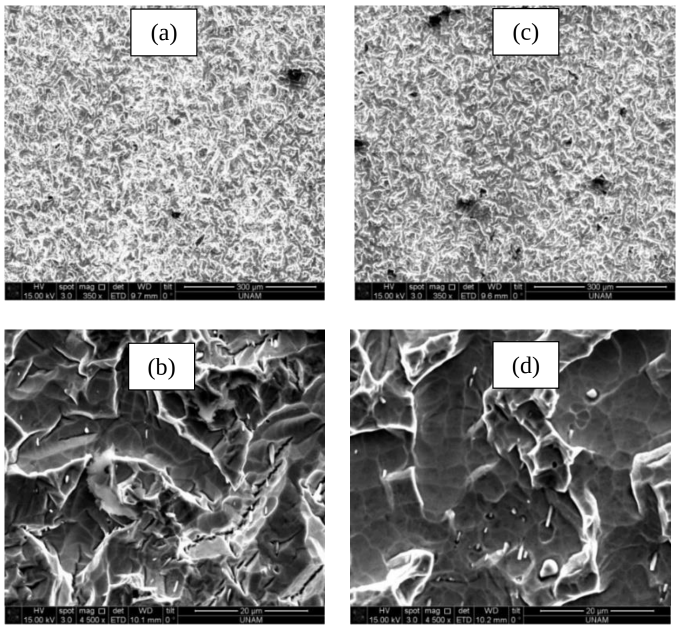

Table 8 Optimum levels of µ-WEDM parameters to obtain minimum the arithmetic surface roughness of the machined surface

Parameters	*d. index = 0.976916*	*PSO*
T_{on} (µs)	5.19697	5.13421
T_{off} (µs)	15.2222	15.15309
I_d (A)	3	3
SV (V)	180	180
R_a (µm)	0.23957	0.23960

3.4 ANOVA and optimisation of µH

The results of the ANOVA of the µH of the machined surface are shown in Table 9. Also, the regression model obtained with 6 DF using the RSM is represented in equation (16). Based on the results of ANOVA, the difference between the R^2 and adj-R^2 was 0.05%, and the adj-R^2 and the predictive R^2 were close enough to show that the predictive capability of the regression model was significant and the experimental and the predicted data were consistent.

$$\begin{aligned}\mu\text{H} = &(-498.3) + 312.45\ T_{\text{on}} + 35.99\ T_{\text{off}} + 7.460\ I_d - 0.535\ \text{SV} - 25.387\ T_{\text{on}}^2 \\ &- 1.9655\ T_{\text{off}}^2 + 0.0775 I_d^2 - 0.000068 SV^2\end{aligned} \quad (16)$$

As shown in Table 9, the p-value and F-value of the model for µH are 0 and 1928.27, respectively, indicating that the regression model was statistically significant. Furthermore, judging from the p-values and F-values of the factors, the T_{on} and I_d were the most significant factors influencing the µH of the Nitinol samples in µ-WEDM, respectively. Additionally, the T_{off} and SV parameters, based on p- and F-values, were equally significant in µH.

Table 9 ANOVA of micro-hardness of the machined surface

Source	*DF*	*Adj SS*	*Adj MS*	*F*	*P*
Regression	8	202148	25268.5	1928.27	0.000
T_{on}	1	64285	64285.3	4905.67	0.000
T_{off}	1	15236	15236.3	1162.70	0.000
I_d	1	1713	1713.5	130.76	0.000
SV	1	157	157.1	11.99	0.003
$T_{on}\times T_{on}$	1	53270	53269.9	4065.07	0.000
$T_{off}\times T_{off}$	1	20803	20803.2	1587.51	0.000
$I_d\times I_d$	1	26	26.3	2.01	0.174
SV×SV	1	0	0.2	0.01	0.909
Pure Error	18	236	13.1		
Total	26	202384			

R^2 = 99.88%, adj-R^2 = 99.83%, pred-R^2 = 99.74%.

Furthermore, the results of the GA optimisation to determine the input parameters that lead to the minimum µH are represented in Figure 9. As shown in this figure, increasing the discharge energy due to an increase in the I_d leads to a monotonic increase of the µH. An increase in the µH of the machined surface was mainly due to the formation of metal oxides on the surface of nitinol alloy (Manjaiah et al., 2015). The presence of oxygen and Cu elements on a typical machined surface originated from the decomposition of the dielectric fluid and the cutting wire, which were confirmed from the EDS results represented in Figure 10(a). Also, the formation of the oxides on the machined surface was confirmed by the XRD analysis represented in Figure 10(b). The formation of the oxide phases and changes in the micro-hardness of the machined surface is highly dependent on machining parameters.

Figure 9 Optimum µ-WEDM parameters to achieve the minimum µH based on GA (d: Composite desirability index) (see online version for colours)

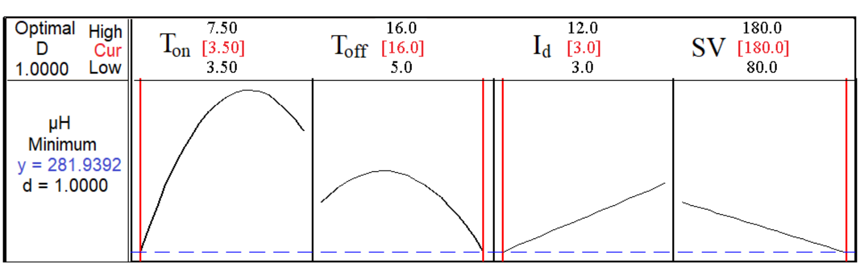

Figure 10 Analyses of machined surface of $Ni_{55.8}Ti$ SMA after the μ-WEDM process under T_{on} = 5 μs, T_{off} = 10 μs, I_d = 11 A and SV = 80 V: (a) electro diffraction spectroscopy and (b) X-ray diffraction spectroscopy

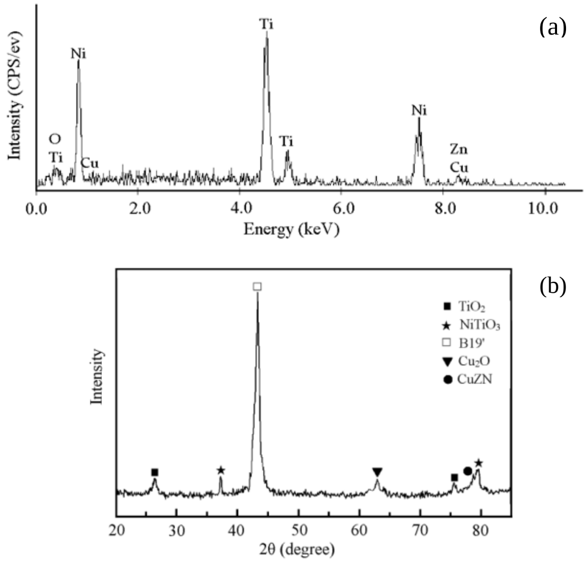

Also, the accumulative results of GA and PSO-optimisation techniques to achieve the minimum μH as well as the results of calculations by replacing these quantities in equation (16) are shown in Table 10. Accordingly, the levels of optimum process parameters and therefore, the results of μH values are identical for both of the optimisation techniques.

Table 10 Optimum levels of μ-WEDM parameters to obtain a minimum micro-hardness of the machined surface

Parameters	*d. index = 1.0*	*PSO*
T_{on} (μs)	3.5	3.5
T_{off} (μs)	16	16
I_d (A)	3	3
SV (V)	180	180
μH, Vikers (kg/mm^2)	281.9392	281.9392

4 Conclusions

The significance of the μ-WEDM process parameters on response variables in the machining of $Ni_{55.8}Ti$ SMA, including the MRR, WLT, SR, and μH, were investigated using Taguchi's L_{27} orthogonal array technique of RSM and ANOVA. Gradient algorithm (GA) and PSO techniques were used to determine the optimum levels of input parameters to obtain the best levels of response variables. The outstanding results of this study are summarised as follows:

1 The most effective parameters on the MRR were SV and T_{off}. The maximum MRR of 0.564 mm^3/min was obtained under T_{on}, T_{off}, I_d, and SV of 7.5 µs, 5 µs, 12, and 115.35 V, respectively. MRR increased monotonically with increasing T_{on} and I_d while it decreased with an increase in T_{off}.

2 The most effective µ-WEDM parameters on the WLT were I_d and SV. The optimal parameters of T_{on}, T_{off}, I_d, and SV to minimise the WLT to 2.052 µm were 3.5 µm, 5 µs, 12 A, 123.43 V, respectively. The WLT increased monotonically with increasing T_{on} while there was an opposite pattern in the case of I_d.

3 The most effective µ-WEDM parameters on the R_a were T_{off} and I_d. The optimal levels of T_{on}, T_{off}, I_d, and SV to achieve the R_a of 0.239 µm were 5.19 µs, 15.22 µs, 3 A 180 V, respectively. The surface roughness decreased monotonically with increasing T_{off} and SV.

4 The T_{on} and I_d were proved as the most significant µ-WEDM parameters on the µH. The levels of T_{on}, T_{off}, I_d, and SV to obtain the minimum µH of 281.94 kg/mm^2, were 3.5 µs, 16 µs, 3 A, and 180 V, respectively. The presence of oxygen and Cu elements, as well as the formation of metal oxides in the white layer, were the primary causes of rising the µH of the machined surfaces.

Acknowledgement

The authors would like to thank the help of Dr. Yiğit Karpat and Dr. Şakir Baytaroğlu at the Micro-System Design and Manufacturing Research Center of Bilkent University for laser topography measurements and µ-WEDM experiments.

References

Agrawal, D.P. and Kamble, D.N. (2019) 'Experimental investigation in photochemical machining process through response surface methodology for manufacturing of micro mould', *International Journal of Mechatronics and Manufacturing Systems*, Vol. 12, pp.116–139.

AL-Anzi, F.S. and Allahverdi, A. (2007) 'A self-adaptive differential evolution heuristic for two-stage assembly scheduling problem to minimize maximum lateness with setup times', *European Journal of Operational Research*, Vol. 182, pp.80–94.

Bai, Q. (2010) 'Analysis of particle swarm optimization algorithm', *Computer and Information Science*, Vol. 3, p.180.

Chaudhari, R., Vora, J.J., Prabu, S.M., Palani, I., Patel, V.K. and Parikh, D. (2019) 'Pareto optimization of WEDM process parameters for machining a NiTi shape memory alloy using a combined approach of RSM and heat transfer search algorithm', *Advances in Manufacturing*, Vol. 9, pp.1–17.

Clerc, M. (1999) 'The swarm and the queen: towards a deterministic and adaptive particle swarm optimization', *Proceedings of the 1999 Congress on Evolutionary Computation-CEC99 (Cat. No. 99TH8406)*, IEEE, Washington, DC, USA, pp.1951–1957.

Daneshmand, S., Kahrizi, E.F. and Ghahi, M.M. (2012) 'Investigation of EDM parameters on surface roughness and MRR of NiTi 60 shape memory alloys', *Australian Journal of Basic and Applied Science*, Vol. 6, pp.218–225.

Dhas, J.E.R. and Kumanan, S. (2011) 'Optimization of parameters of submerged arc weld using non conventional techniques', *Applied Soft Computing*, Vol. 11, pp.5198–5204.

ES-Souni, M., ES-Souni, M. and Fischer-Brandies, H. (2002) 'On the properties of two binary niTi shape memory alloys. effects of surface finish on the corrosion behaviour and in vitro biocompatibility', *Biomaterials*, Vol. 23, pp.2887–2894.

Fourie, P. and Groenwold, A.A. (2002) 'The particle swarm optimization algorithm in size and shape optimization', *Structural and Multidisciplinary Optimization*, Vol. 23, pp.259–267.

Guo, Y., Klink, A.F.U.C. and Snyder, J. (2013) 'Machinability and surface integrity of nitinol shape memory alloy', *CIRP Annals*, Vol. 62, pp.83–86.

Hsieh, S., Chen, S., Lin, H., Lin, M. and Chiou, S. (2009) 'The machining characteristics and shape recovery ability of Ti–Ni–X (X= Zr, Cr) ternary shape memory alloys using the wire electro-discharge machining', *International Journal of Machine Tools and Manufacture*, Vol. 49, pp.509–514.

Júnior, J.D.A.B., Nunes, M.V.A., Nascimento, M.H.R., Leite, J.C., Rodriguez, J.L.M., De Freitas, C.A.O., Júnior, M.F., De Oliveira, E.F., De Alencar, D.B. and Moraes, N.M. (2018) 'Multi-objective optimization techniques to solve the economic emission load dispatch problem using various heuristic and metaheuristic algorithms', *Optimization and Control of Electrical Machines*, p.13.

Kalmar, M., Boese, A., Maldonado, I., Landes, R. and Friebe, M. (2019) 'NITINOL-based actuator for device control even in high-field MRI environment', *Medical Devices (Auckland NZ)*, Vol. 12, p.285.

Kumar, V., Kumar, V. and Jangra, K.K. (2015) 'An experimental analysis and optimization of machining rate and surface characteristics in WEDM of Monel-400 using RSM and desirability approach', *Journal of Industrial Engineering International*, Vol. 11, pp.297–307.

Lotfineyestanak, A.A. and Daneshmand, S. (2013) 'The effect of operational cutting parameters on Nitinol-60 in wire electrodischarge machining', *Advances in Materials Science and Engineering*.

Magabe, R., Sharma, N., Gupta, K. and Davim, J.P. (2019) 'Modeling and optimization of wire-EDM parameters for machining of Ni 55.8 Ti shape memory alloy using hybrid approach of Taguchi and NSGA-II', *The International Journal of Advanced Manufacturing Technology*, Vol. 102, pp.1703–1717.

Majumder, A., Das, P.K., Majumder, A. and Debnath, M. (2014) 'An approach to optimize the EDM process parameters using desirability-based multi-objective PSO', *Production and Manufacturing Research*, Vol. 2, pp.228–240.

Manjaiah, M., Narendranath, S., Basavarajappa, S. and Gaitonde, V. (2015) 'Effect of electrode material in wire electro discharge machining characteristics of Ti50Ni50 – xCux shape memory alloy', *Precision Engineering*, Vol. 41, pp.68–77.

Mu, X., Zhou, M., Yao, S. and Yang, J. (2018) 'High efficient electrical discharge machining by servo voltage adaptive control', *Procedia CIRP*, Vol. 68, pp.654–659.

Puri, A.B. (2017) 'Advancements in micro wire-cut electrical discharge machining', *Non-Traditional Micromachining Processes*, Springer, Cham.

Rathi, P., Ghiya, R., Shah, H., Srivastava, P., Patel, S., Chaudhari, R. and VORA, J. (2019) 'Multi-response optimization of Ni55. 8Ti shape memory alloy using Taguchi–grey relational analysis approach', *Recent Advances in Mechanical Infrastructure: Proceedings of ICRAM 2019*, Springer, Singapore, p.13.

Roy, A.K. and Kumar, K. (2014) 'Effect and optimization of various machine process parameters on the surface roughness in EDM for an EN41 material using grey-Taguchi', *Procedia Materials Science*, Vol. 6, pp.383–390.

Shabgard, M., Oliaei, S.N.B., Seyedzavvar, M. and Najadebrahimi, A. (2011) 'Experimental investigation and 3D finite element prediction of the white layer thickness, heat affected zone, and surface roughness in EDM process', *Journal of Mechanical Science and Technology*, Vol. 25, pp.3173–3183.

Sharma, N., Raj, T. and Jangra, K.K. (2017) 'Parameter optimization and experimental study on wire electrical discharge machining of porous Ni40Ti60 alloy', *Proceedings of the Institution of Mechanical Engineers, Part B: Journal of Engineering Manufacture*, Vol. 231, pp.956–970.

Soni, H., Sannayellappa, N. and Rangarasaiah, R.M. (2017) 'An experimental study of influence of wire electro discharge machining parameters on surface integrity of TiNiCo shape memory alloy', *J. Mater. Res.*, Vol. 32, pp.3100–3108.

Upadhyay, L., Aggarwal, M. and Pandey, P.M. (2019) 'Experimental investigations into rotary magnetic field and tool assisted electric discharge machining using magneto rheological fluid as dielectric', *International Journal of Mechatronics and Manufacturing Systems*, Vol. 12, pp.1–19.

Wadood, A. (2016) 'Brief overview on nitinol as biomaterial', *Advances in Materials Science and Engineering*, pp.1–9.